Reduced Graphene Oxide Coated Iridium Oxide as a Catalyst for Alkaline Water Electrolysis

Student Name: Ziqing Zuo

School: Kang Chiao International School East Campus

Province: Jiangsu

Country: China

Name of Supervisor: Macdona Masali

Job title: high school chemistry teacher

School: Kang Chiao International School East Campus

Province: Jiangsu

Country: China

Abstract

Producing hydrogen by water electrolysis has attracted significant attention as a potential renewable energy solution. In this work, a catalyst with reduced graphene oxide (rGO) loaded on IrO_2/TiO_2 (called $rGO/IrO_2/TiO_2$) was designed for catalytic oxygen evolution reaction (OER). The catalyst was synthesized by coating graphene oxide onto an IrO_2/TiO_2 precursor pretreated, followed by thermal treatment at 450 °C to achieve reduction and adhesion of graphene to the substrate. Benefiting from the synergistic effect of rGO, IrO_2, and TiO_2 matrix, the $rGO/IrO_2/TiO_2$ catalyst only needs an overpotential of 240 mV, 320 mV to reach 10 mA cm^{-2} and 100 mA cm^{-2} in the OER. Its morphology and crystalline structure were characterized by SEM and XRD spectroscopy, and its electrochemical performance was tested by LSV analysis, EIS impedance spectrum, and double-layer capacitance (C_{dl}) measurements. This work introduces an innovative and eco-friendly strategy for simultaneously constructing a high-performance, functionalized Ir-based catalyst.

Keywords:

Graphene, Iridium oxide, Water electrolysis, Alkaline, Oxidation evolution reaction, Electrocatalyst.

Table of Contents

1. Introduction

Currently, fossil fuels are the primary sources of hydrogen production due to their efficiency and cost-effectiveness.[1] However, with the rising demand for hydrogen as a purely clean energy source and growing concerns about the environmental impact of fossil fuels, such as global warming, it becomes imperative to develop sustainable and economical methods for large-scale hydrogen production.[1] Currently, hydrogen produced by electrocatalytic water splitting using sustainable electricity is considered to be an ideal alternative energy source because it is pollution-free and carbon-free in both the production and utilization stages. [2]

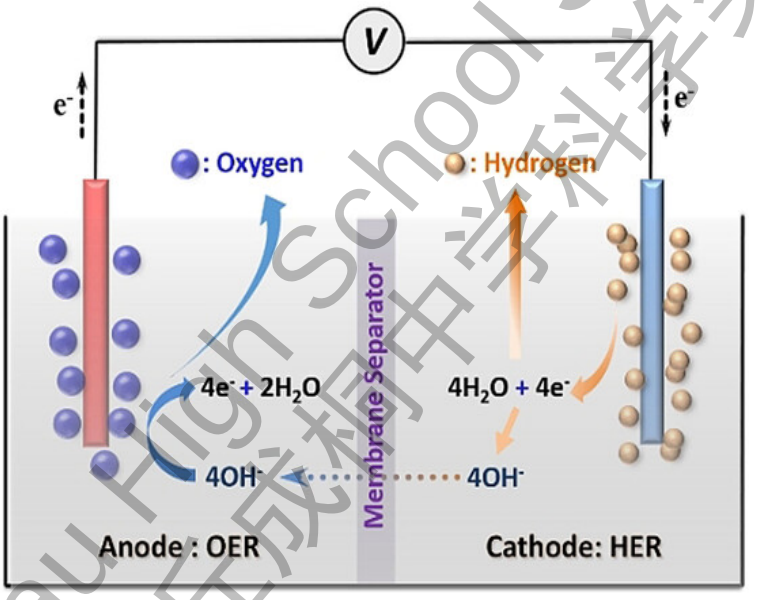

Scheme 1: A typical water electrolysis cell under alkaline. [4]

As shown in Equation (1), Water electrolysis, or water splitting, is an endothermic reaction and has a ΔG of 237.1 kJ mol^{-1} under standard conditions (25 °C, 101.325 kPa), indicating a non-spontaneous process. As Scheme 1 shows, water electrolysis involves two half-reactions: the hydrogen evolution reaction (HER) at the cathode and the oxygen evolution reaction (OER) at the anode. Under alkaline conditions, one of the most popular electrolysis conditions, the water molecules at the cathode gain electrons to produce hydrogen, and the remaining hydroxide anions transport to the anode to lose electrons and produce oxygen, as shown in Equation [(2) and (3)].[3]

$$\text{Water splitting: } 2H_2O(l) \rightarrow 2H_2(g) + O_2(g) \quad (1)$$

In alkaline electrode:

$$\text{HER: } 2H_2O(l)+4e^-\rightarrow 2H_2(g)+4OH^- \quad (2)$$

$$\text{OER: } 4OH^-\rightarrow O_2(g)+2H_2O(l)+4e^- \quad (3)$$

HER entails 2-electron transfer, while OER necessitates 4-electron transfer, which requires the reaction to surmount a higher energy barrier. Consequently, individuals are dedicated to discovering exceptional OER electrocatalysts to lower the energy barrier of water electrolysis.[5] Under standard conditions, the theoretical potential to run the water electrolysis reaction is 1.23 V (0 V for HER and 1.23 V for OER, vs. RHE). However, the actual voltage required for water electrolysis is much higher than the theoretical value due to energy barriers associated with the electrochemical kinetics and mass transport in the cell, resulting in some resistance in the system. High activation energies for HER and OER lead to extra voltage demands, known as overpotential. Therefore, the actually applied potential for water electrolysis (E_{ap}) can be concluded in Equation (4), where η_{HER} and η_{OER} are the overpotentials and R_{system} is the voltage drops due to system resistances.

$$E_{ap} = 1.23\ V + \eta_{HER} + \eta_{OER} + R_{system} \quad (4)$$

To reduce the overpotential of OER, many chemists have attempted to develop high-efficiency OER catalysts, such as noble metals Pt, Ru, Ir, and Pd and their oxides, as well as some transition metal-based alloys such as Ni-Fe, Ni-Cu, Ni-Mo, Ni-Ir, and Co-Fe.[6] Currently, the Ir-based catalysts are considered promising due to their excellent OER performance and stability.[7] However, there is still room to further enhance its electrocatalytic performance. For improvement, Zhang et al. synthesized a Ru@Ir-O catalyst by introducing a core-shell nanostructure with oxygen bound to the Ir shell, leading to an increase in activity, resulting in an extremely low OER overpotential of 238 mV (at 10 mA cm^{-2}). [8] Zhu et al. prepared the Ir-Co_3O_4 catalyst by doping dispersed Ir atoms into spinel Ir-Co_3O_4. The introduction of Ir single atoms increases electronic conductivity and decreases the adsorption energy barrier, resulting in an overpotential of 236 mV (at 10 mA cm^{-2}).[9]

Besides enhancing the intrinsic activity of electrocatalysts, increasing the number of active sites—regions on the surface of a catalyst that adsorb and desorb reactants to catalyze the reaction—can also improve the OER performance, as demonstrated by measuring the Electrochemical Surface Area (ECSA). [10] Reduced graphene oxide (rGO), a material with an exceptional surface area and electrical conductivity, can provide more catalytic active sites. [11] Moreover, despite the nitrogen gas reduction process eliminating oxygen-containing functional groups from graphene oxide (GO) and creating large defect regions that enhance electron transfer, carbonyl groups (C=O) at the edges of GO nanosheets may still remain and serve as active sites by adsorbing intermediate species for water splitting. [12] These properties make rGO a promising material for further enhancing the OER catalysts. Huang et al. developed an rGO-coated Ni_3Se_2 catalyst on nickel foam, denoted as rGO/Ni_3Se_2/NF, providing abundant active sites due to the rGO integration and demonstrating excellent OER and HER performance with low overpotentials of 292.61 mV and 251.01 mV, respectively, at ±10 mA cm^{-2}. [13] Bhosale et al. developed a vanadium oxide-reduced graphene oxide-nickel oxide (VrG/NiO) electrocatalyst, which utilizes active sites at the interface of V_2O_5, rGO, and NiO to achieve efficient oxygen evolution reaction (OER) performance with a low overpotential of 155.47 mV at 10 mA cm^{-2}. [14]

Even though they have achieved good performance, the potential benefits of integrating rGO and IrO_2 have yet to be fully realized.

Herin, a reduced graphene oxide (rGO)-coated IrO_2 catalyst on TiO_2 (denoted as rGO/IrO_2/TiO_2) was designed by solution coating and then calcination at 450 ºC for catalytic oxygen evolution reaction (OER). Through the synergetic effect of rGO and IrO_2, the overpotential decreases to 240 mV and 320 mV at 10 mA cm^{-2} and 100 mA cm^{-2} in the OER, respectively. Accordingly, it exhibits a low Tafel slope and large double-layer capacitance (C_{dl}) values. It is noteworthy that the graphene coating enhanced the performance of the IrO_2/TiO_2 catalyst, but it does not work on the nickel foam electrode. This work highlights the impact of rGO on IrO_2 for the OER performance, providing innovative insight for developing highly efficient Ir-based catalysts.

2. Experimental Methods

2.1 Chemicals

Table 1: The name, standard, and manufacturer of the chemicals.

Name	Standard	Manufacturer
KOH	AR	RHAWN
Distilled water	1-10μs/cm	Metal and Minerals Trading Corporation of India
N_2 (g)	99.999%	Metal and Minerals Trading Corporation of India
Ti plate	10*10*0.1cm^3	Jiangsu Tishida Metal Technology
Graphene oxide	AR	Metal and Minerals Trading Corporation of India
$H_2IrCl_6 \cdot 6H_2O$	AR	Johnson Matthey
$H_2C_2O_4$	industrial	Tongliao
$CH_3CH_2CH_2OH$	AR	MACKLIN
Pt electrode	1	Chinstrument
Hg/HgO electrode	1	Chinstrument

2.2 Instrument

Table 2: The name, standard, and manufacturer of the instruments.

Name	Model	Manufacturer
Analytical balance	KHW-EX	Kunhong
Atmosphere Furnace	JC202	Jingang Industrial Furnace Technology (Suzhou)
Pipette	100-1000μl	LICHEN
Pipette tips	1000μl	Yangzhou Jiazhe Experimental Instrument
Brush	#3	Mui Ho Mui Metal Processing
Electrochemical workstation	CHI660E	Chinstrument
Magnetic stirrer	MSC	JOANLAB
Manual plate shears	XL-6	Xianglong

2.3 Synthesis of IrO_2/TiO_2

First, a solution of 1-propanol and chloroiridinic acid with a mass ratio of 14:1 was prepared and stirred thoroughly by a magnetic stirrer (15 min). Using a pipette and an analytical balance, 0.3 g of this solution was added to a 10×10×0.1 cm^3 Ti plate that had been acid-pickled (30 min), and it was spread evenly on the plate by using a brush that had dipped in the same solution. After the solution was dried, the plate was calcined in the atmosphere furnace at 450 ºC for 2 hours. This process was repeated another 4 times on the same Ti plate as it could allow the IrO_2 to be more evenly distributed and make fewer cracks between IrO_2 particles on the plate. Additionally, the surface of the Ti plate produced titanium dioxide during the calcination. As a result, an IrO_2 catalyst with approximately 1.0 mg/cm^2 of Ir was synthesized. The detailed schematic illustration of the synthesis procedure is depicted as Step 1 in Scheme 2.

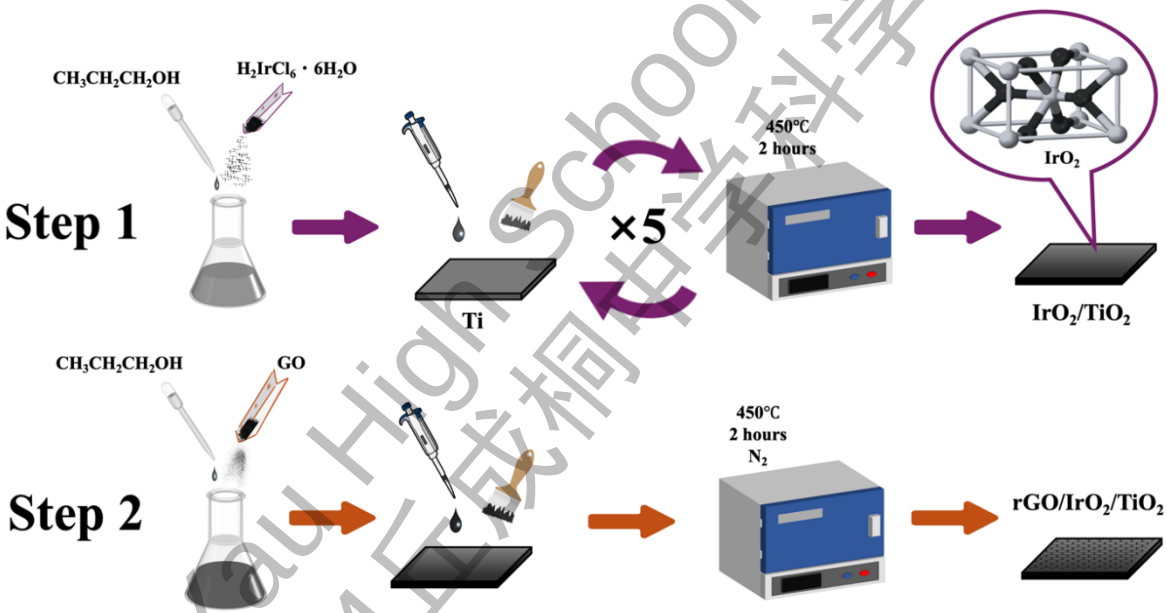

Scheme 2: the schematic procedure of $rGO/IrO_2/TiO_2$ synthesis.

2.4 Synthesis of $rGO/IrO_2/TiO_2$

Another solution of 1-propanol and graphene oxide powder with a mass ratio of 11:1 was prepared and stirred thoroughly by a magnetic stirrer (15 min). Next, 0.3 g of this solution was added to the IrO_2/TiO_2 and was applied evenly using a brush that had dipped in the same solution. After the solution was dried, the plate was calcined in nitrogen at 450 ºC for 2 hours, ensuring that the GO was reduced successfully. After that, the synthesis of $rGO/IrO_2/TiO_2$ with approximately 0.2

mg/cm^2 of graphene was finished (Step 2 in Scheme 2), and both the IrO_2/Ti and the rGO/IrO_2/TiO_2 were sliced into 1×1.5×0.1 cm^3 to prepare for the experiment.

2.5 Synthesis of rGO/NF

As an excellent non-precious metal catalyst, nickel foam is used to develop outstanding non-expensive catalysts. Therefore, reduced graphene oxide is also coated on the nickel foam using a similar method with rGO/IrO_2/TiO_2, serving as a control sample. All four synthesized catalysts are shown in Figure 1.

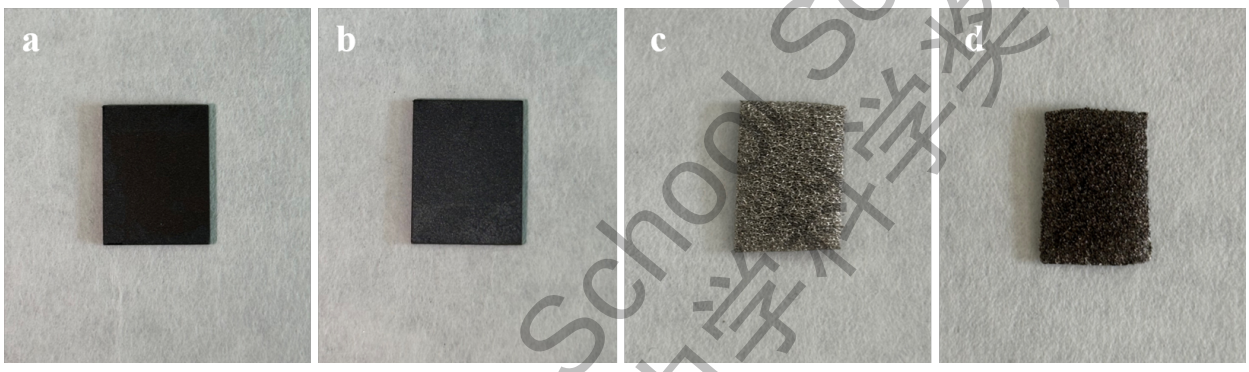

Figure 1: Photographs of (a) rGO/IrO_2/TiO_2; (b) IrO_2/TiO_2; (c) NF; and (d) rGO/NF.

2.6 Characterization Methods

The structural analysis and crystalline phase purity of all samples were examined by the X-ray diffraction (XRD) on a Panalytical Empyrean diffractometer utilizing Cu Kα radiation spectra (λ=1.54 Å, 300 W) in the 2θ range of 20-80°. Furthermore, scanning electron microscopy (SEM) and energy dispersive spectroscopy (EDS) mapping are performed for structural morphologies and elemental analysis at 5 kV using Tescan MAIA3 XMH (15 kV).

2.7 Electrochemical Measurements

The electrochemical performance of the proposed catalysts and NF was evaluated using the electrochemical workstation CH Instrument Ins (CHI 660). A conventional three-electrode setup was employed, consisting of a Pt foil as the counter electrode, an Hg/HgO reference electrode (0.098V vs. SHE), and rGO/IrO_2/TiO_2 and IrO_2/TiO_2 as the working electrodes for all electrochemical measurements. The catalytic activity was assessed in a 1 M KOH electrolyte

(pH=14) at room temperature (25 ºC). The working potential of the samples was converted from E(V vs. SHE) to E(V vs. RHE) using the Nernst equation — Equation (5):

$$E_{(V\ vs\ RHE)} = E^{\theta}_{Hg/HgO} + E_{Hg/HgO} + 0.059 \times pH - iR. \quad (5)$$

The $E^{\theta}_{Hg/HgO}$ is 0.098V, the $E_{Hg/HgO}$ is the measured potential, and the pH is 14. In addition, the current (i/A) was converted into current density (j/mA cm^{-2}). All polarization curves were corrected by iR compensation.

3. Results and Discussion

3.1 Material Characterizations

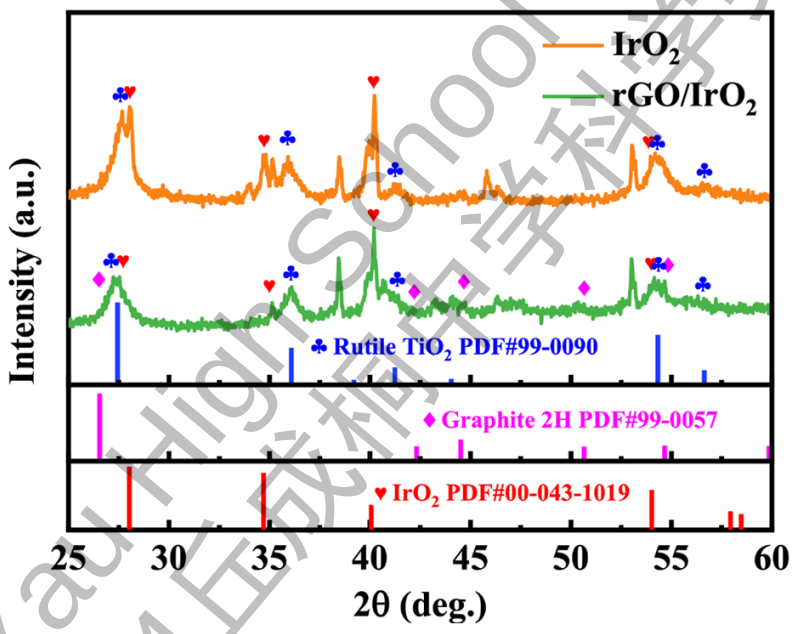

Figure 2: XRD analysis of catalyst IrO_2/TiO_2 and $rGO/IrO_2/TiO_2$

As shown in Figure 2, the phase structure and crystallinity of catalyst IrO_2/TiO_2 and $rGO/IrO_2/TiO_2$ were investigated through XRD. The XRD spectra of the catalyst IrO_2/TiO_2 demonstrate characteristic peaks at 28.04°, 34.79°, 40.19°, and 53.99°, matching the (110), (101), (200), and (211) planes of the IrO_2 (PDF#00-043-1019), respectively. Likewise, the XRD spectra of the catalyst $rGO/IrO_2/TiO_2$ demonstrate characteristic peaks at 27.64°, 35.06°, 40.14°, and 54.11°, also matching the (110), (101), (200), and (211) planes of the IrO_2 (PDF#00-043-1019), respectively. This indicates that both catalysts contain IrO_2. The XRD spectra of the catalyst

IrO_2/TiO_2 also demonstrate characteristic peaks at 27.62, 35.98, 41.20, 54.28, and 56.63, matching the (110), (101), (111), (211), and (220) of the Rutile TiO_2 (PDF#99-0090), respectively. Similarly, the XRD spectra of the catalyst $rGO/IrO_2/TiO_2$ demonstrate characteristic peaks at 27.31, 36.09, 41.24, 54.37, and 56.65, matching the (110), (101), (111), (211), and (220) of the Rutile TiO_2 (PDF#99-0090), respectively. This suggests that the surfaces of the Ti plates have oxidized to TiO_2. However, only the XRD spectra of the catalyst $rGO/IrO_2/TiO_2$ demonstrate little characteristic peaks at 26.66, 42.15, 44.60, 50.65, and 54.73, corresponding to the (002), (100), (101), (102), and (004) of the graphite (PDF#00-043-1019), respectively. This justifies the coated rGO in the catalyst.

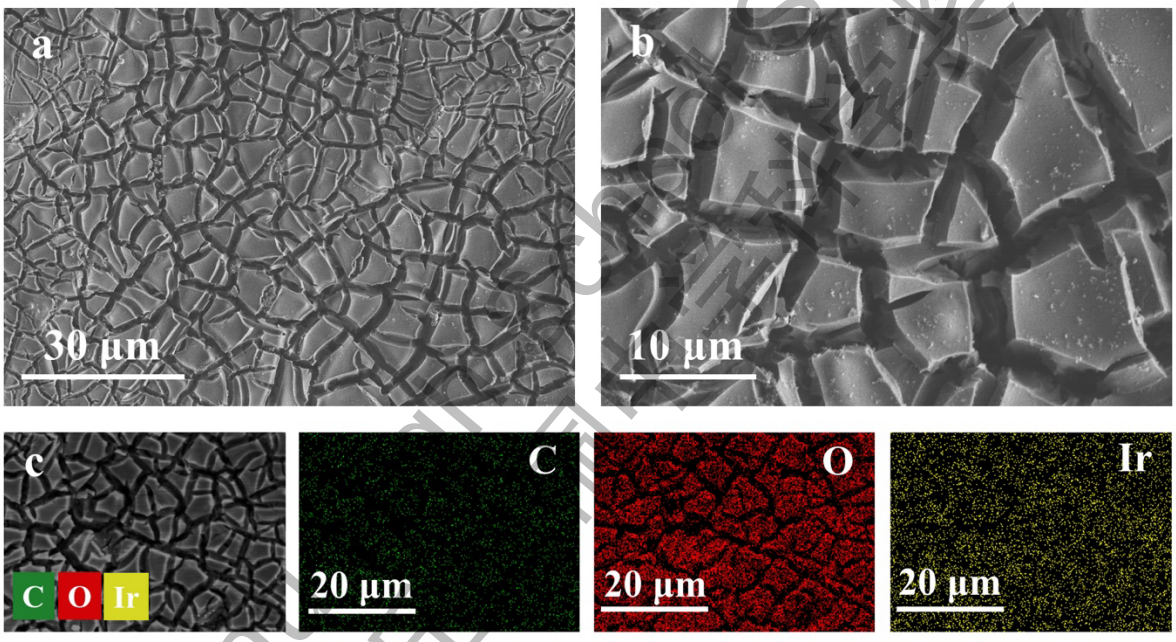

Figure 3: Morphology and structure characterizations. (a, b) SEM images of IrO_2/TiO_2 at different magnifications; (c) EDS mappings of IrO_2/TiO_2.

The surface morphologies of IrO_2/TiO_2 and $rGO/IrO_2/TiO_2$ were examined using a scanning electron microscope (SEM). As illustrated in Figures 3a and 3b, the SEM images of the IrO_2/TiO_2 at varying magnifications exhibit a distinctive cracked mud-like structure. The surface is observed to be textured and composed of numerous interconnected polygonal platelets with distinct boundaries. At higher magnification (Figure 4b), it can be observed that the platelets mentioned above exhibit smooth surfaces, with the presence of small particulates dispersed across them.

Figure 3c presents the Energy Dispersive X-ray Spectroscopy (EDS) mappings of the IrO_2/TiO_2, which demonstrate the elemental distribution across the surface. The EDS results indicate the presence of iridium (Ir) and oxygen (O) distributed uniformly throughout the electrode surface by the cracked pattern observed in the SEM images. It is noteworthy that a minor quantity of carbon (C) has also been identified, which may be attributed to the carbonization of the organic components of chloroplatinic acid, leaving behind carbon-based residues.

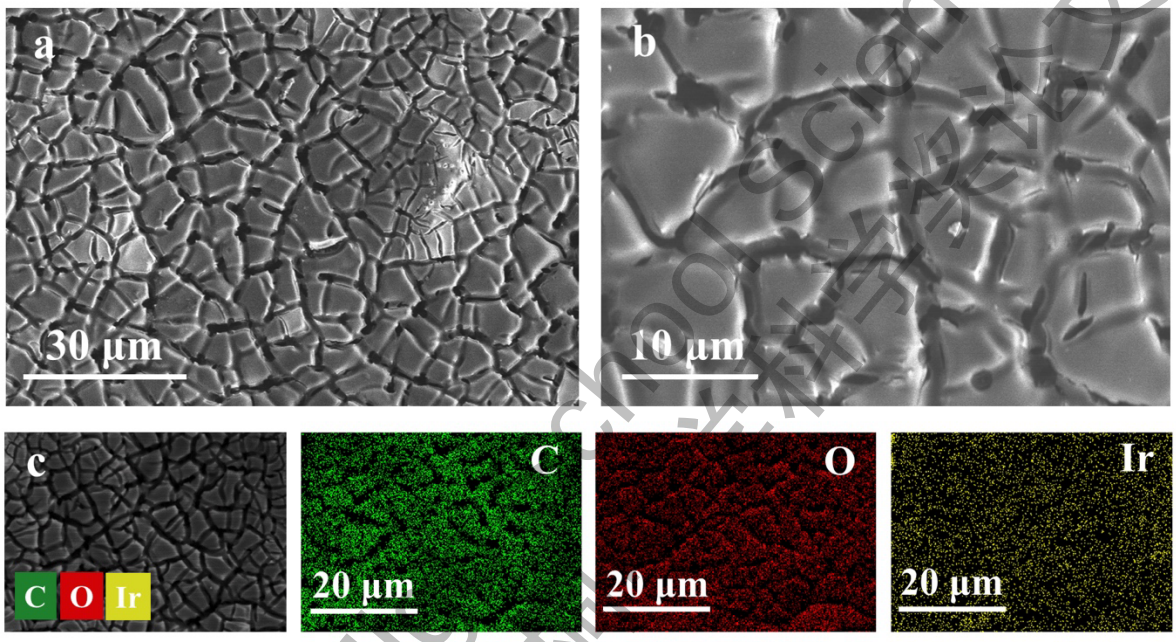

Figure 4: Morphology and structure characterizations. (a, b) SEM images of $rGO/IrO_2/TiO_2$ at different magnifications; (c) EDS mappings of $rGO/IrO_2/TiO_2$.

Figures 4a and 4b present the SEM images of the $rGO/IrO_2/TiO_2$ at different magnifications for comparison. The surface morphology of the $rGO/IrO_2/TiO_2$ displays a comparable cracked mud-like structure to that of IrO_2/TiO_2, yet with discernible distinctions. The edges of the polygonal platelets exhibit a slight degree of smoothness and definition, indicative of a thin graphene layer coating the IrO_2 structure. At higher magnification (Figure 4b), the surface of the platelets displays a more textured appearance relative to the IrO_2/TiO_2, which may be attributed to the graphene coating.

As illustrated in Figure 4c, the EDS mappings of the rGO/IrO_2/TiO_2 provide insight into the elemental composition following the graphene coating process. In addition to Ir and O, there is a notable increase in the carbon signal, which is discernible and distributed uniformly across the surface. This result corroborates the successful deposition of the graphene layer on the IrO_2/TiO_2. Consequently, the distribution of Ir, O, and C appears to be uniform and follows the pattern of the cracked electrode surface.

Scanning electron microscopy (SEM) imaging revealed a distinct cracked mud-like structure for both catalysts, with the rGO/IrO_2/TiO_2 exhibiting a smoother surface texture, indicative of the graphene coating. Energy-dispersive X-ray spectroscopy (EDS) mapping further confirmed the successful deposition of the graphene layer on the IrO_2/TiO_2 surface. While the overall cracked mud-like structure is maintained, the graphene coating introduces subtle changes to the surface texture and significantly increases the carbon content of the electrode. These structural modifications likely play a crucial role in the enhanced electrocatalytic properties observed in the rGO/IrO_2/TiO_2, as discussed in the subsequent sections.

3.2 Electrocatalytic Properties

A conventional three-electrode electrochemical system was employed to assess the electrocatalytic oxygen evolution reaction (OER) activity of the resulting catalyst in an alkaline solution to ascertain the electrocatalytic performance. Figure 5a shows the linear sweep voltammetry curves of each sample. It can be observed that the OER catalytic activity of the IrO_2-based catalyst is significantly enhanced after coating the graphene layer, where its overpotentials at 10 and 100 $mA \cdot cm^{-2}$ are only 240 mV and 320 mV, respectively, compared to 320 mV and 400 mV of the original IrO_2 catalyst at the same current density. However, the OER catalytic activity of the NF-based electrode is undermined after coating the graphene layer, which has overpotentials of 460 mV and 640 mV at 10 and 100 $mA \cdot cm^{-2}$, respectively.

Figure 5b shows the Tafel slope of each tested electrode. It demonstrates that the rGO/IrO_2/TiO_2 has the smallest value of 53.81 $mV \cdot dec^{-1}$, which is less than IrO_2/TiO_2's 82.93 $mV \cdot dec^{-1}$. The lower Tafel slope indicated a more rapid reaction kinetics and a more favorable OER mechanism. On the other side, the rGO/NF electrode has the highest value (148.81 $mV \cdot dec^{-1}$) of Tafel slope,

which is much higher than the NF electrode's 84.72 mV·dec^{-1}, indicating a worse electrocatalytic performance after coating graphene on nickel foam.

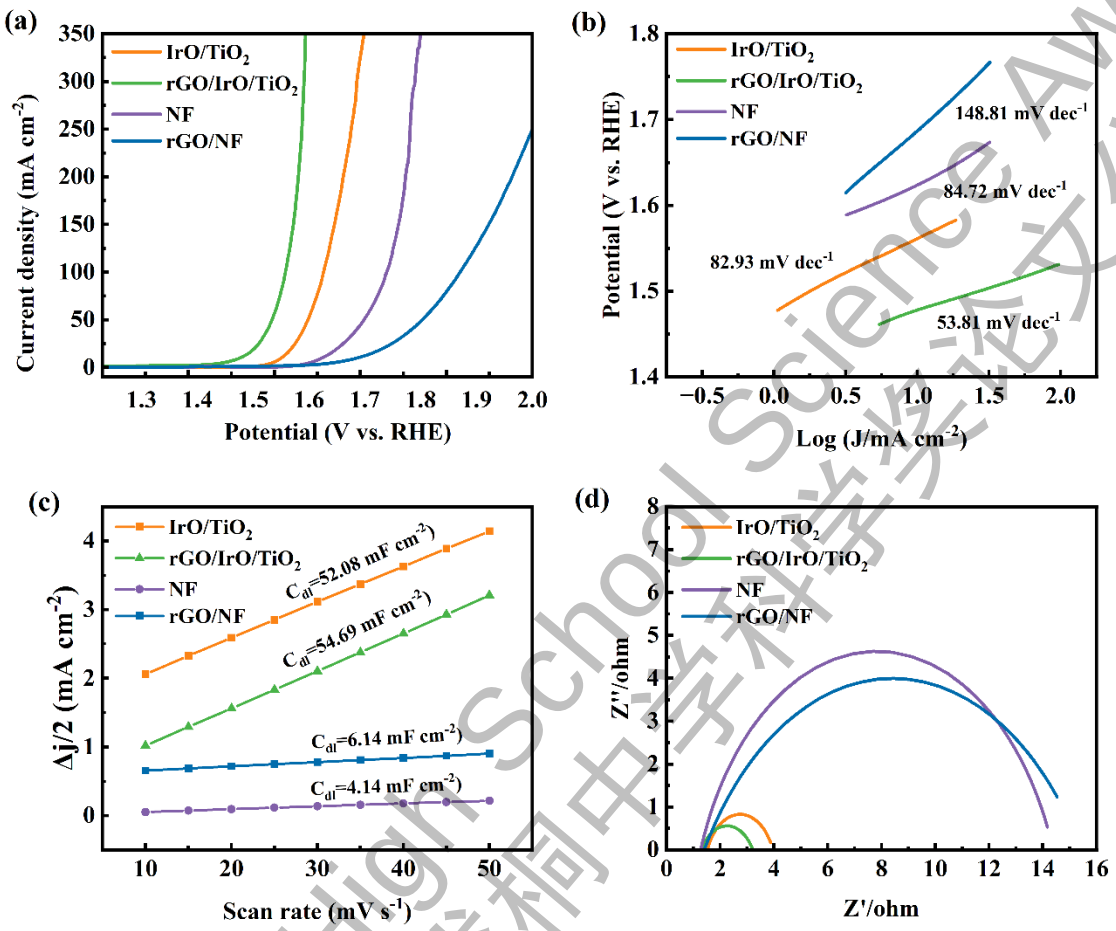

Figure 5: (a) Polarization curves and (b) corresponding Tafel plots in 1.0 M KOH electrolyte; (c) C_{dl} values and (d) EIS Nyquist plots of IrO_2/TiO_2, $rGO/IrO_2/TiO_2$, NF, and rGO/NF.

Figure 5c shows the capacitive current densities as a function of the scanning rate for each electrode, which was extracted from the CV curves tested. The result illustrates that the C_{dl} of the $rGO/IrO_2/TiO_2$ is 54.69 mF·cm^{-2}, higher than the IrO_2/TiO_2's 52.08 mF·cm^{-2}. Likewise, the C_{dl} of the rGO/NF electrode (6.14 mF·cm^{-2}) is higher than the NF electrode's value of 4.14 mF·cm^{-2}. Both cases prove that graphene coating on electrode materials can increase their active sites, a core measurement of the electrocatalytic property.

Moreover, the kinetics of the OER process can be more accurately elucidated through electrochemical impedance measurement. Figure 5d shows that the impedance of $rGO/IrO_2/TiO_2$

is much smaller than that of IrO_2/TiO_2, while NF's impedance is larger than rGO/NF's, indicating a faster charge transfer ability and quicker reaction kinetics when coating graphene on IrO_2.

It is noteworthy that while the graphene coating enhanced the performance of the IrO_2/TiO_2 catalyst, it had a deleterious impact on the nickel foam electrode. This observation highlights the necessity of meticulous consideration of material combinations in catalyst design, as the same modification can yield markedly disparate outcomes on disparate substrates.

The electrochemical measurements showed that the $rGO/IrO_2/TiO_2$ catalyst exhibits superior performance. The enhanced performance of the $rGO/IrO_2/TiO_2$ catalyst can be ascribed to several contributing factors. The incorporation of rGO is believed to augment the overall electrical conductivity of the catalyst, thereby facilitating accelerated electron transfer during the OER process. The interaction between rGO and IrO_2 may create beneficial synergistic effects, potentially altering the electronic structure of the active sites and optimizing the adsorption energies of reaction intermediates. The elevated surface area of rGO furnishes supplementary active sites for the OER, as substantiated by the augmented C_{dl} value. Moreover, the graphene coating may safeguard the underlying IrO from degradation, thereby enhancing the catalyst's long-term stability.

4. Conclusion

In summary, this study demonstrates a promising strategy for enhancing the performance of Ir-based OER catalysts through the integration of reduced graphene oxide. The surface morphology of the $rGO/IrO_2/TiO_2$ exhibits a comparable cracked mud-like structure, with a uniform dispersion of graphene across the surface. The $rGO/IrO_2/TiO_2$ catalyst demonstrates exceptional catalytic activity. It only needs an overpotential of 240 mV to reach 10 mA cm^{-2} and 320 mV to reach 100 mA cm^{-2} in the OER and has the smallest Tafel slope of 53.81 $mV \cdot dec^{-1}$. Its double-layer capacitance (C_{dl}) is 54.69 $mF \cdot cm^{-2}$, which further illustrates its large electrochemically active surface area. These findings contribute to the ongoing efforts to develop high-performance catalysts for water electrolysis and provide valuable insights for future research in this field.

Acknowledgment:

Selected Topic:

The idea for this topic was initiated by the author, who initially identified the topic of graphene-enhanced electrolysis of water for hydrogen production through the news about Green Hydrogen and what he had learned about graphene in the school's chemistry class. The final topic was then determined through communication with the supervisor.

Experiment:

The entire process was done independently by the author himself during the synthesis of catalysis. The supervisor provided basic assistance during the electrochemical workstation experiments, such as operating techniques, steps, and principles behind the operation. The experiments were conducted in the laboratory of Northeastern University, China. The XRD and SEM characterizations were tested at the Analytical Testing Center, College of Science, Northeastern University, China.

Some experiment pictures:

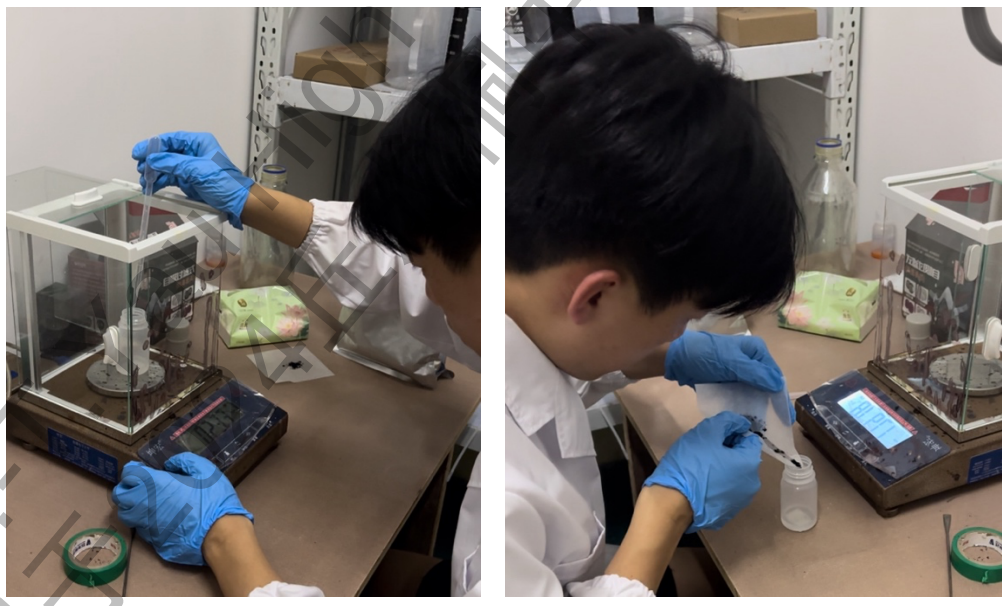

S1: Preparing the solution of graphene oxide.

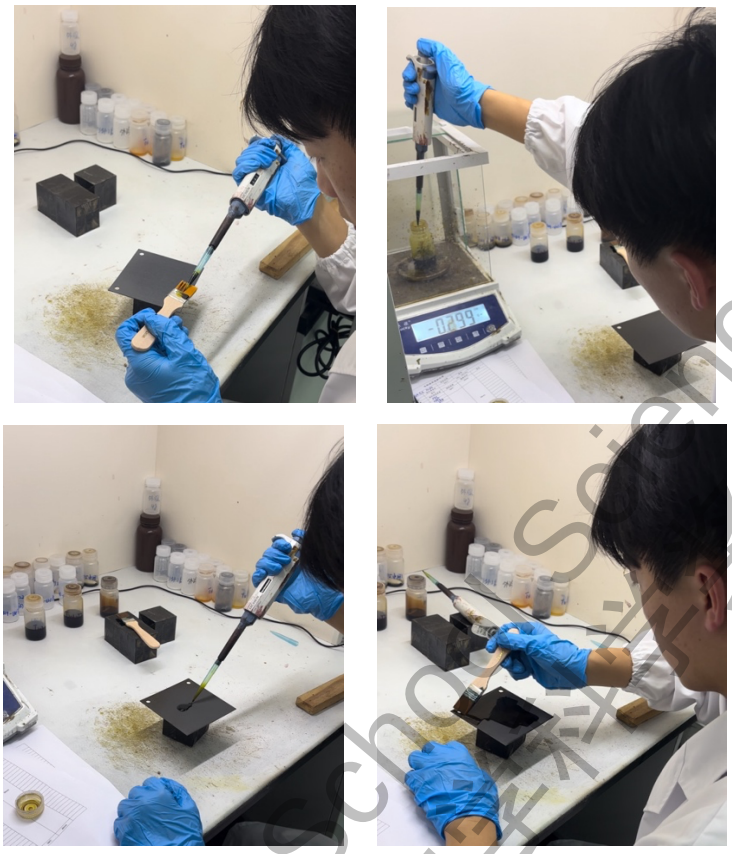

S2: Brushing the solution to the Ti plate.

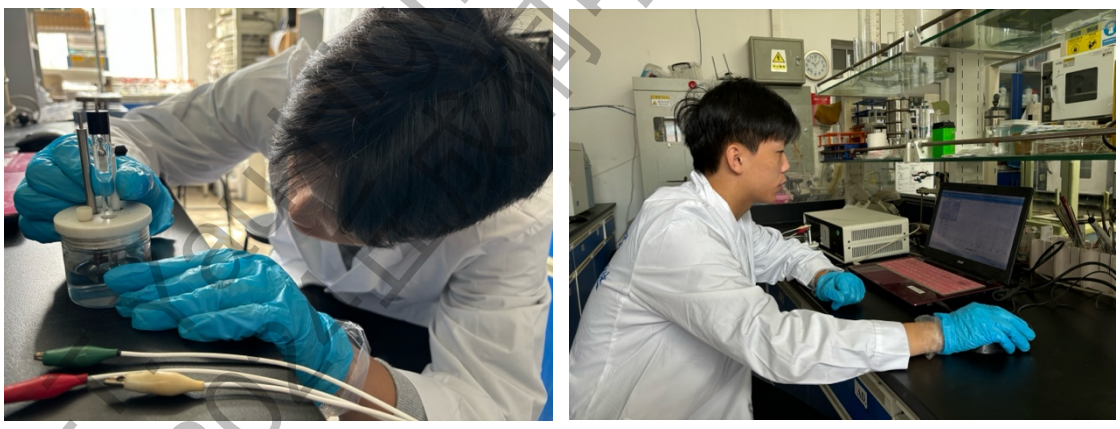

S3: Testing the electrochemical performance.

Thesis writing:

The supervisor assisted with basic writing structure and techniques, Jade XRD analysis, and Origin drawing. All the guidance was unpaid.

References

1. Jamadar, A.S.; Rohit Sutar; Patil, S.; Khandekar, R.; Yadav, J.B. Progress in Metal Oxide-Based Electrocatalysts for Sustainable Water Splitting. *Materials Reports Energy* **2024**, *4*, 100283–100283.

2. Panchenko, V.A.; Daus, Yu.V.; Kovalev, A.A.; Yudaev, I.V.; Litti, Yu.V. Prospects for the Production of Green Hydrogen: Review of Countries with High Potential. *International Journal of Hydrogen Energy* **2022**, *48*, 4551-4571.

3. Badgett, A.; Ruth, M.; Pivovar, B. Economic Considerations for Hydrogen Production with a Focus on Polymer Electrolyte Membrane Electrolysis. *Elsevier eBooks* **2022**, 327–364.

4. Yu, M.; Budiyanto, E.; Tüysüz, H. Principles of Water Electrolysis and Recent Progress in Cobalt-, Nickel-, and Iron-Based Oxides for the Oxygen Evolution Reaction. *Angewandte Chemie International Edition* **2022**, *61*, e202103824.

5. Andrés Parra-Puerto; Ying, K.; Fahy, K.F.; Goode, A.E.; Ryan, M.P.; Kucernak, A. Supported Transition Metal Phosphides: Activity Survey for HER, ORR, OER, and Corrosion Resistance in Acid and Alkaline Electrolytes. *ACS Catalysis* **2019**, *9*, 11515–11529.

6. Wang, Y. Recent Advanced Study of Novel Electrode Materials. *Advances in Analytical Chemistry* **2021**, *11*, 200–216.

7. Qin, R.; Chen, G.; Feng, X.; Weng, J.; Han, Y. Ru/Ir-Based Electrocatalysts for Oxygen Evolution Reaction in Acidic Conditions: From Mechanisms, Optimizations to Challenges. *Advanced Science* **2024**, *11*, 2309364.

8. Zhang, J.; Fu, X.; Xia, F.; Zhang, W.; Ma, D.; Zhou, Y.; Peng, H.; Wu, J.; Gong, X.; Wang, D.; et al. Core-Shell Nanostructured Ru@Ir–O Electrocatalysts for Superb Oxygen Evolution in Acid. *Small* **2022**, *18*, 2108031.

9. Zhu, Y.; Wang, J.; Koketsu, T.; Kroschel, M.; Chen, J.-M.; Hsu, S.-Y.; Henkelman, G.; Hu, Z.; Strasser, P.; Ma, J. Iridium Single Atoms Incorporated in Co_3O_4 Efficiently Catalyze the Oxygen Evolution in Acidic Conditions. *Nature Communications* **2022**, *13*, 7754.

10. Huang, C.-J.; Xu, H.-M.; Ting-Yu Shuai; Zhan, Q.-N.; Zhang, Z.-J.; Li, G.-R. A Review of Modulation Strategies for Improving Catalytic Performance of Transition Metal Phosphides for Oxygen Evolution Reaction. *Applied catalysis. B, Environmental (Print)* **2023**, *325*, 122313–122313.

11. Yang, P.; Yang, X.; Liu, W.; Guo, R.; Yao, Z. Graphene-Based Electrocatalysts for Advanced Energy Conversion. *Green Energy & Environment* **2022**, *8*, 1265-1278.

12. D. Amaranatha Reddy; Choi, J.-S.; Lee, S.-H.; Ma, R.; Tae Kyu Kim Self-Assembled Macro Porous ZnS–Graphene Aerogels for Photocatalytic Degradation of Contaminants in Water. *RSC Advances* **2015**, *5*, 18342–18351.

13. Huang, S.-J.; Balu, S.; Nazar Riswana Barveen; Sankar, R. Surface Engineering of Reduced Graphene Oxide onto the Nanoforest-like Nickel Selenide as a High Performance Electrocatalyst for OER and HER. *Colloids and Surfaces A Physicochemical and Engineering Aspects* **2022**, *654*, 130024–130024.

14. Mrunal Bhosale; Sadhasivam Thangarasu; Magdum, S.S.; Jeong, C.; Oh, T.-H. Enhancing the Electrocatalytic Performance of Vanadium Oxide by Interface Interaction with RGO and NiO Nanostructures for Electrochemical Water Oxidation. *International Journal of Hydrogen Energy* **2024**, *54*, 1449–1460.